Journal of Materials Chemistry A

PAPER

View Article Online
View Journal | View Issue

Cite this: J. Mater. Chem. A, 2019, 7, 10739

The complex defect chemistry of antimony selenide†

Christopher N. Savory *[ab] and David O. Scanlon *[abc]

Antimony selenide, Sb_2Se_3, is a highly promising solar absorber material with excellent optoelectronic properties; solar cell efficiencies are now poised to exceed 10%, after a rapid rise over the past few years. However, the open-circuit voltage (V_{oc}) of most cells remains low, and such a high V_{oc} deficit, along with defect spectroscopy studies, suggest that recombination *via* deep trap states may be a limiting factor. A comprehensive study of all the intrinsic defects in Sb_2Se_3 is warranted – in this article, we calculate the formation energies and transition levels of these defects using hybrid Density Functional Theory. Our results demonstrate that cation–anion antisite defects have low formation energies, and possess multiple mid-gap transition levels, making them the most likely candidates for previously observed trap states, and possible recombination centres. Suppressing these dominant defects will be crucial for future cell development – thus we also present potential methods to counteract their detrimental effects and allow further improvement in efficiencies.

Received 22nd February 2019
Accepted 2nd April 2019

DOI: 10.1039/c9ta02022e

rsc.li/materials-a

1 Introduction

Photovoltaics (PV) have developed over the past few decades as one of the most promising sustainable energy generation technologies available, and as the cost of cells and modules continues to decrease, parity in $ per W with fossil fuels at utility scale becomes ever more achievable.[1] Still, alternative architectures beyond traditional silicon-based panels, such as building-integrated PV or flexible devices, as well as diversification of materials should be considered to further enable widespread usage of photovoltaics in the future. Established thin-film technologies such as CdTe and Cu(In, Ga)Se_2 are well situated to be used in such devices,[2] however the drawbacks of scarcity and expense (for In and Te) or toxicity (Cd) remain concerns for large-scale deployment. As such, emergent thin film solar absorbers remain of significant scientific and economic interest.[3]

Antimony selenide, Sb_2Se_3, possesses a number of optimal properties for use as a solar absorber: a near-ideal 1.2 eV to 1.3 eV band gap, strong optical absorption, a binary stoichiometry (simplifying synthesis), and its pseudo-one-dimensional crystal structure has been proposed to demonstrate significantly reduced grain-boundary recombination in comparison with traditional absorbers due to a lack of dangling bonds.[4] Prior theoretical calculations have reaffirmed the optimal band gap and absorption,[5,6] while calculation of thin-film efficiency metrics have demonstrated particularly high and promising values for Sb_2Se_3, even for very thin layers of material.[7,8] Prior to the past few years, Sb_2Se_3 was most of interest for use in 'extremely thin absorber' (ETA) cells, as a sensitizer to TiO_2, however efficiencies remained near 3%.[9–12] Over the past five years, however, creation of heterojunction cells, with careful control of growth conditions to align the Sb_2Se_3 chains perpendicular to the substrate, and optimization of the junction interface has rapidly improved cell performance, with a recently published record efficiency of 9.2%,[13] cementing it as a highly promising PV material. Additionally, as devices fabricated using techniques such as closed-space sublimation (CSS) or rapid thermal evaporation (RTE) that retain efficiencies above 5% further demonstrate the potential scalability of the technology.[4,8,14]

Nevertheless, a common theme through both ETA and heterojunction Sb_2Se_3 cells has been a relatively large V_{oc} deficit: despite its 1.3 eV optimal band gap, many cells demonstrate V_{oc} below 0.4 V[4,15] and the record published V_{oc} is 0.45 V.[8] If Sb_2Se_3 is to breach 10% efficiency and become a competitive solar absorber, this deficit must be addressed: while some improvement is likely to be possible through choice of contacts, the possibility of deep defects enabling high levels of Shockley–Read–Hall (SRH) recombination is a significant concern, especially in light of the detection of multiple trap states through Deep-level Transient Spectroscopy (DLTS), as published by Tang and co-workers.[16] Previous theoretical studies by Tumelero *et al.*[17] and

[a]University College London, Department of Chemistry, 20 Gordon Street, London WC1H 0AJ, UK. E-mail: christopher.savory.14@ucl.ac.uk; d.scanlon@ucl.ac.uk

[b]Thomas Young Centre, University College London, Gower Street, London WC1E 6BT, UK

[c]Diamond Light Source Ltd., Diamond House, Harwell Science and Innovation Campus, Didcot, Oxfordshire OX11 0DE, UK

† Electronic supplementary information (ESI) available: Lattice parameter comparison, theoretical defect formalism, thermodynamic transition levels. See DOI: 10.1039/c9ta02022e

Liu *et al.*[18] have examined the defect properties of the antimony chalcogenides, however they have done so using Density Functional Theory (DFT), employing standard functionals which require corrections to the band gap, and can also incorrectly describe the underlying defect physics,[19] and they do not include certain, crucial defects. In this article, we present theoretical defect calculations performed with hybrid DFT to enable a complete picture of the intrinsic defect chemistry of Sb_2Se_3, identify potential detrimental trap states, and discuss their implications for the future of the material as a solar absorber.

2 Computational methods

All calculations were performed using periodic density functional theory within the Vienna Ab Initio Simulation Package (VASP), using scalar relativistic PAW pseudopotentials.[20–23] The structure of Sb_2Se_3, as well as the elemental phases of Sb and Se, were relaxed using the HSE06 hybrid DFT functional,[24] with the addition of the D3 Grimme dispersion correction[25] to account for the interactions between the chains in the pseudo-1D structure of Sb_2Se_3. This method has been previously shown to give highly accurate structural properties in comparison with experiment, and also results in a predicted band gap that lies within 10 meV of a 0 K Varshni fit to experimental measurements.[8,26] Defect calculations were also performed using the HSE06+D3 method on a $1 \times 3 \times 1$ supercell (60 atoms) with a Γ centered $2 \times 2 \times 2$ *k*-point mesh and a plane-wave energy cutoff of 350 eV. All structures were optimized until the forces on each atom were below 0.02 eV $Å^{-1}$. Spin–orbit coupling effects were not included in these calculations due to their expense and minimal structural effects; the relativistic renormalisation at the *k*-points considered is also small (~0.05 eV). A comprehensive description of the defect formation formalism is given in the ESI.† To account for the 'finite size effects' of the supercell and restore the dilute defect model, three corrections were used. Firstly, a correction is necessary to ensure that the electrostatic potential of the host and defect supercells are aligned.[27] Secondly, defects within supercells may interact with their own periodic images, causing the formation of a defect band; if this defect level is shallow, it may interact with a conduction or valence band, leading to erroneous filling with electrons and affecting the total energy – to counteract this, a 'band filling' correction is applied.[28] Thirdly, charged defects may interact with each other coloumbically, due to the long range behaviour of such effects, and so a further 'image charge' correction is required. In this report, we use the formalism of Murphy *et al.*, as this accounts for anisotropy in the dielectric constant of the material, an effect which is strong for Sb_2Se_3.[29] All transition levels are included in Tables 2 and 3 of the ESI,† and all optimized supercell structures are provided in an online repository (https://github.com/SMTG-UCL/Sb2Se3_intrinsic_defects). The VESTA program was used for the visualization and figures of the Sb_2Se_3 crystal structure.[30]

3 Results

Sb_2Se_3 has no stable competing phases, and so its chemical potential space is solely bounded by the elements and its own formation enthalpy (−1.495 eV); the chemical potential (μ) limits are thus given by the Sb-rich (A, $\mu_{Sb} = 0$ eV) and Se-rich (B, $\mu_{Se} = 0$ eV) extremes. The transition level (TL) diagrams of Sb_2Se_3, calculated using the HSE06+D3 method described in the Computational methods, are depicted for these two chemical potential limits in Fig. 2. Individual sites are marked by subscripts after the atom label, and reference the positions marked in the labelled crystal structure depicted in Fig. 1. In both diagrams, it is clear that calculating defects for all possible sites is necessary, but especially for Se, as their behaviour can differ significantly – this can be rationalised by the very different local environments for each Se position. Under Sb-rich conditions, there are numerous defects with formation energies under 1.5 eV, and thus are likely to be present in the sample in reasonable concentrations, including V_{Se} (all sites), Sb_{Se} (all sites) and the Sb interstitial. In this instance, the dominant defects are $V_{Se,2}$ and $Sb_{Se,1}$, which will compensate each other at a Fermi level ~0.58 eV above the valence band maximum (VBM), and pin the Fermi level at that point. At this position, all of the above defects will be present, and all possess deep transition levels: all three V_{Se}, regardless of site, act as deep donors (as also seen in both PBE studies)[17,18] while all three Sb_{Se} are amphoteric, with the (+1/−1) transition level of $Sb_{Se,1}$ and (+3/−1) of $Sb_{Se,3}$ standing out as a possible trap states for both holes and electrons. This amphoteric behaviour was not explored in either of the previous studies, yet appears to be crucial to the understanding of this defect – both in its potential pinning effect on the Fermi level, and with a mid-gap transition level, possibility to act as a site of efficient SRH recombination.

In the Se-rich regime, however, many of these previously problematic defects are moved to higher formation energies.

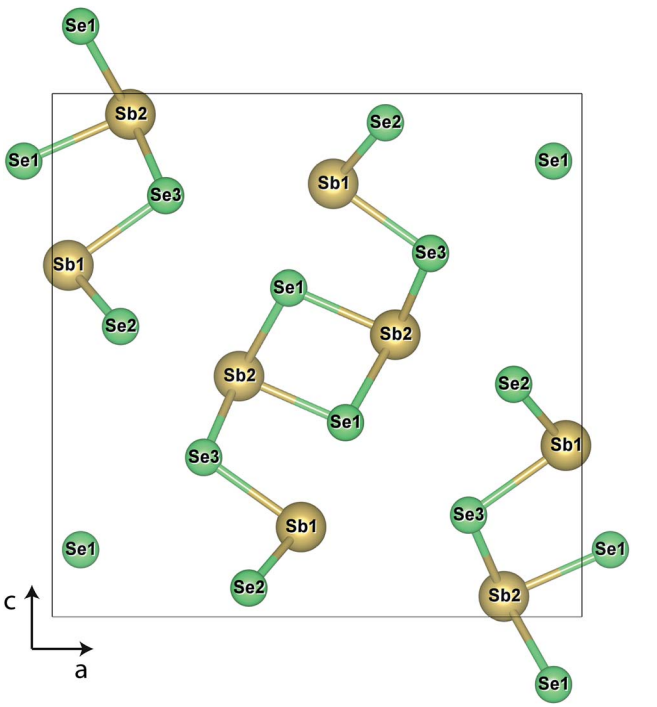

Fig. 1 Crystal structure of Sb_2Se_3, with individual site labels. Antimony atoms are depicted in gold and selenium in light green.

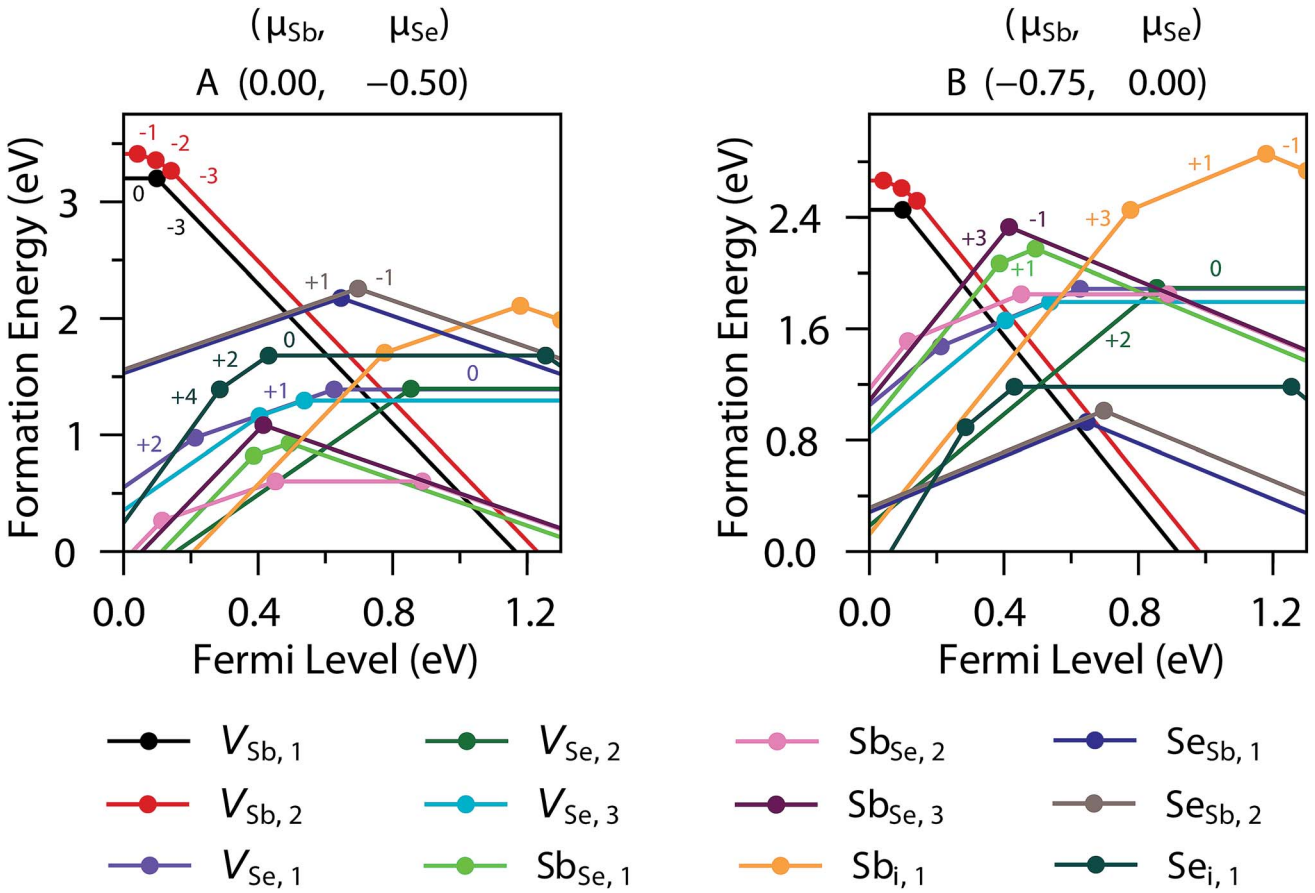

Fig. 2 Defect transition level diagram for Sb_2Se_3 under limiting chemical potential conditions ((A) Sb-rich; (B) Se-rich), plotting defect formation energy (eV) against position of Fermi level above the VBM. Defect labels are given in the legend, charge states are given by labels adjacent to lines, with lines of the same slope representing the same charge state, and transition levels are represented by the filled dots.

While the neutral charge states of both V_{Sb} remain high in formation energy, the −3 charge states are relevant elsewhere in the Fermi level range – they intercept the +1 charge states for each Se_{Sb} antisite in the middle of the gap; again these will act to compensate each other and likely pin the Fermi level mid-gap (~0.62 eV above the VBM). For this Fermi level position, far fewer defects have a formation energy below 1.5 eV: only the Se_{Sb} and V_{Sb} already noted, in addition to the Se interstitial. Of these, Se_i has multiple transition levels deep within the band gap, that could plausibly act as hole or electron traps. V_{Sb} acts as a deep acceptor, with all transition levels lying close to, but further than 0.025 eV from, the VB edge; the separation by site reveals that the −2 and −1 charge states are stabilised for $V_{Sb,2}$, which has a more regular coordination environment, compared to $V_{Sb,1}$, where only the (−3/0) transition level is observed. Both Se_{Sb} defects however, are amphoteric, with an ultra-deep (+1/−1) transition level; lying in the middle of the gap, these are particularly likely to act as recombination centres, as they will likely have similar carrier capture cross-sections for both electrons and holes, and thus are potentially highly detrimental to photovoltaic performance.

To attempt to validate some of these results, we can compare the positions of these expected trap states with those found in a recent DLTS study of Tang and co-workers on cells produced by RTE and vapour transport deposition;[16] in both cases, the traps were observed to appear in similar positions albeit with different densities. Comparing to the vapour transport deposition values first, the two hole traps lie at 0.48 ± 0.07 eV and 0.71 ± 0.02 eV above the valence band maximum – these align almost exactly with our calculated HSE06+D3 (+1/−1) TLs of $Sb_{Se,1}$ (VBM + 0.494 eV) and $Se_{Sb,2}$ (VBM + 0.697 eV) respectively. A similar agreement is found with the RTE-synthesised cell DLTS values too (the hole traps lying at 0.49 ± 0.03 eV and 0.74 ± 0.04 eV above the valence band maximum) and these are represented pictorially in the Fig. 3. A recent study found that variation of ionization energies with temperature can cause disparities between defect transition levels and the actual likely activation energies seen in experimental DLTS studies in GaN (highly dependent on the defect itself – for 300 K, a variation of ~60 meV was seen for V_{Ga}–O_N–2H, while a significant ~250 meV shift was seen for C_N),[31] and as such this agreement between our simulations and DLTS could be fortuitous. In both prior, PBE-based defect studies of Sb_2Se_3, however, no transition levels align well with these DLTS levels, even considering a large temperature effect (neither study gives a possible hole trap within 0.3 eV of the 0.71 eV hole trap position, and the

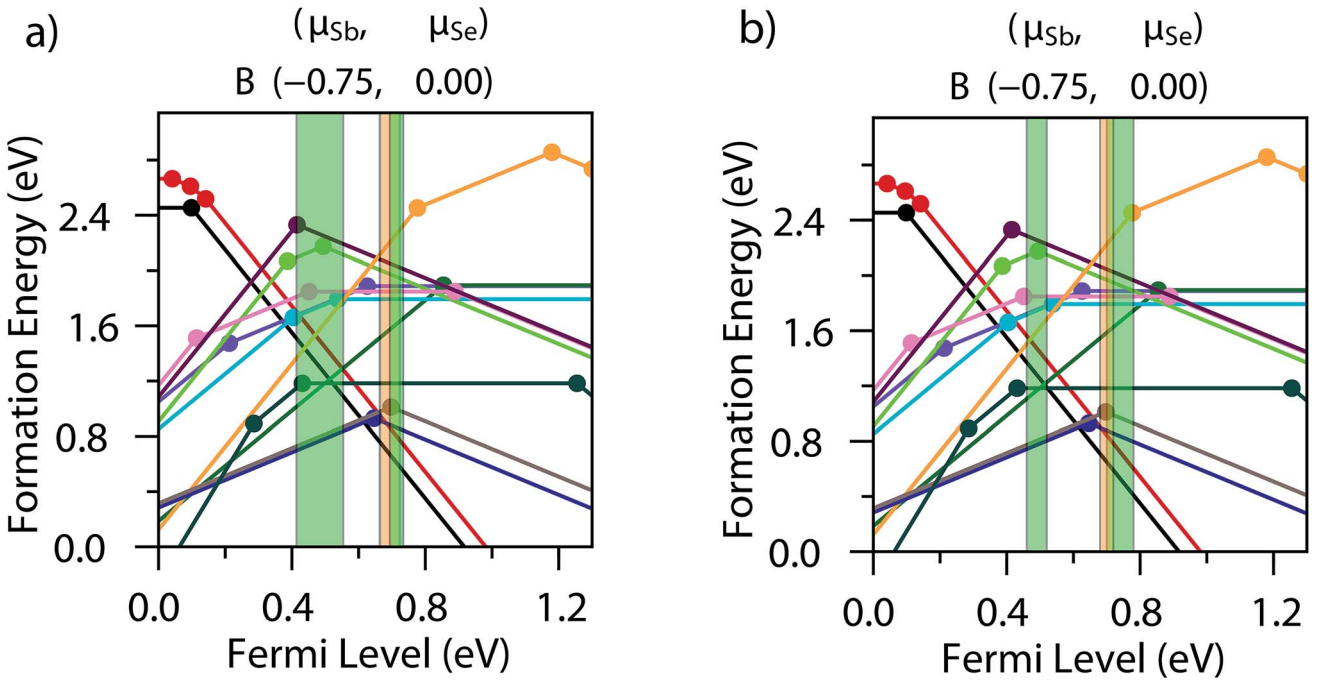

Fig. 3 Defect transition level diagrams for Sb_2Se_3 with the position of the DLTS trap levels recorded by Wen *et al.* for (a) a VTD-synthesised and (b) a RTE-synthesised cell marked on, with the experimental uncertainty given by the bar width.[16] Green bars represent the hole traps, and orange represents the electron trap, and the defect labels are identical to those in Fig. 2. The diagram is plotted at the Se-rich chemical potential limit, in accordance with Wen *et al.*'s expected synthesis conditions, however the actual chemical potential conditions during synthesis are difficult to determine and likely to be closer to stoichiometry than our extreme limits – as such, the formation energies are only loosely considered when identifying the trap states.

closest transition levels are at least 0.1 eV from the first hole trap) – this does seem to demonstrate the necessity for a hybrid functional, as well as a comprehensive study of all possible charge states to properly describe the material's complex defect chemistry. A recent study has found that even hybrid DFT energies, if based on defect geometries relaxed using standard DFT functionals, can lead to significant uncertainty in the defect level.[19] For the electron trap (E1), a further level of uncertainty is introduced through the renormalization of the conduction band position with temperature – however, using the calculated gap of 1.300 eV for the position of the conduction band minimum (CBM) the trap (0.61 ± 0.03 eV below the CBM) is predicted to lie at essentially the same position as the second hole trap (H2), and as an amphoteric defect, $Se_{Sb,2}$ (CBM – 0.603 eV) is the most likely candidate for this trap also. The proposition that these may in fact be the same defect state is not too unlikely – its position near the middle of the gap could lead to very similar capture cross-sections for both holes and electrons,[32] and E1 and H2 were found to have similar concentrations to each other for both sampled cells. While it is clear further validation may be necessary, both cation–anion and anion–cation intrinsic antisites seem to be the strongest candidates for the trap states in Sb_2Se_3, given our calculations.

4 Discussion

The identification of potential recombination centres at both chemical potential limits has implications not only for the use of Sb_2Se_3 as a solar absorber but also other applications that might utilise its high absorption, but also need specific purity, such as radiation detection. The detrimental effect of these trap states could be alleviated, however, by targeted passivation: an analogy might be made to another popular, earth abundant solar absorber, Cu_2ZnSnS_4 (CZTS), which had plateaued in efficiency due to a large V_{oc} deficit – which some studies have related partly to intrinsic antisite defects or cation disorder, with varying reports of Cu_{Zn}, Cu_{Sn} or Sn_{Zn}.[33–35] Some improvement in CZTS cells has been observed, however, through targeted doping with Na, suppressing the effect of intrinsic defects, and increasing carrier lifetimes.[36–38] For Sb_2Se_3, a possible strategy may be to favour Se-rich synthesis or treatments, combined with extrinsic doping on the Sb sites to suppress the formation of Se_{Sb} defects.

Alternatively, we might note that the multiple deep acceptors and donors in both chemical potential limits suggest that Sb_2Se_3 will resist significant p or n-type doping, and that a more effective cell may be possible through synthesising Sb_2Se_3 as close to stoichiometry as possible, resulting in a compromise that maximises the formation of both antisite defects, and forming a p–i–n architecture with Sb_2Se_3 as an intrinsic layer. In this case, efforts may be necessary to find optimal contact materials to account for the limited accessible range in Fermi level.

As well as their potential impact on the photovoltaic behaviour of Sb_2Se_3, the presence of low formation energy, deep antisite defects bears discussion within the wider context of

defects in functional energy materials. With the rise of the hybrid lead halide perovskites in PV, a number of publications have discussed the topic of 'defect tolerance'[39–41] in semiconductors, whereby materials are resistant to the formation of defects within them, or that such defects' detrimental effects are minimised. Some studies have directly linked defect tolerance with an electronic structure that has a VBM of antibonding character[39,40] (demonstrated in materials with ns^2 'lone pair' cations such as Pb^{2+}, Sb^{3+} or Bi^{3+})[42–45] and a high dielectric constant. In our previous work, we found Sb_2Se_3 to possess both of these characteristic properties,[8] however this study, along with the V_{oc} deficit in cells, suggests that Sb_2Se_3 is far from defect tolerant. This is consistent with recent research suggesting that defect tolerance has significant dependence on other factors, such as crystal structure and cation valence.[46,47] On the other hand, from a chemist's point of view, the presence of such cation–anion antisites in Sb_2Se_3 is perhaps not surprising – the amphoteric, 'soft' chemical behaviour of both antimony and selenium is well known, and thus the relative stability of such antisites, and multiple charge states therein, might naively be expected to be possible. Indeed, previous studies in the chemically-related bismuth tetradymite structures (Bi_2Se_3, Bi_2Se_2Te) found that cation–anion antisite defects were also low in formation energy and could act as limits to performance.[48] Regardless, it is clear that close investigation of the defect behaviour of Sb_2Se_3 is necessary for its future usage in energy applications.

5 Conclusions

In this study, we have calculated the intrinsic defects in the candidate solar absorber Sb_2Se_3 using hybrid Density Functional Theory and including all defect sites to attempt to perform a complete assessment of its defect behaviour. We have found that, regardless of chemical potential limit, there will be low formation energy cation–anion anisite defects with mid-gap transition levels that could act as recombination centres. By noting the alignment of our calculated transition levels with published DLTS results, we propose that these Se_{Sb} and Sb_{Se} defects are most likely to be the trap states present in devices, and the potential barrier to improving device efficiencies. In order for Sb_2Se_3 to further improve as a useful optoelectronic material, it is critical that these defects must be suppressed, perhaps through targeted passivation by extrinsic dopants.

Conflicts of interest

There are no conflicts of interest to declare.

Acknowledgements

The authors would like to thank Dr Ben Williamson and Dr John Buckeridge for useful discussions. The authors acknowledge the use of the UCL Legion and Grace High Performance Computing Facility (Legion@UCL and Grace@UCL) in the production of this work. This work was also performed on the ARCHER UK National Supercomputing Service, *via* our membership of the UK's HEC Materials Chemistry Consortium, funded by EPSRC (EP/L000202). CNS is grateful to the Department of Chemistry at UCL for the provision of a DTA studentship (ref no. 1492829). DOS acknowledges support from the SUPERSOLAR Solar Energy Hub (EP/J017361/1), EPSRC (EP/N01572X/1), and membership of the Materials Design Network.

References

1 N. M. Haegel, R. Margolis, T. Buonassisi, D. Feldman, A. Froitzheim, R. Garabedian, M. Green, S. Glunz, H.-M. Henning, B. Holder, I. Kaizuka, B. Kroposki, K. Matsubara, S. Niki, K. Sakurai, R. A. Schindler, W. Tumas, E. R. Weber, G. Wilson, M. Woodhouse and S. Kurtz, *Science*, 2017, **356**, 141–143.
2 L. M. Peter, *Philos. Trans. R. Soc., A*, 2011, **369**, 1840–1856.
3 A. M. Ganose, C. N. Savory and D. O. Scanlon, *Chem. Commun.*, 2017, **53**, 20–44.
4 Y. Zhou, L. Wang, S. Chen, S. Qin, X. Liu, J. Chen, D.-J. Xue, M. Luo, Y. Cao, Y. Cheng, E. H. Sargent and J. Tang, *Nat. Photonics*, 2015, **9**, 409–415.
5 M. R. Filip, C. E. Patrick and F. Giustino, *Phys. Rev. B: Condens. Matter Mater. Phys.*, 2013, **87**, 205125.
6 J. J. Carey, J. P. Allen, D. O. Scanlon and G. W. Watson, *J. Solid State Chem.*, 2014, **213**, 116–125.
7 B. Blank, T. Kirchartz, S. Lany and U. Rau, *Phys. Rev. Appl.*, 2017, **8**, 024032.
8 L. J. Phillips, C. N. Savory, O. S. Hutter, P. J. Yates, H. Shiel, S. Mariotti, L. Bowen, M. Birkett, K. Durose, D. O. Scanlon and J. D. Major, *IEEE J. Photovolt.*, 2018, **9**, 544–551.
9 S. Messina, M. T. S. Nair and P. K. Nair, *J. Electrochem. Soc.*, 2009, **156**, H327–H332.
10 S.-J. Moon, Y. Itzhaik, J.-H. Yum, S. M. Zakeeruddin, G. Hodes and M. Grätzel, *J. Phys. Chem. Lett.*, 2010, **1**, 1524–1527.
11 N. Guijarro, T. Lutz, T. Lana-Villarreal, F. O'Mahony, R. Gómez and S. A. Haque, *J. Phys. Chem. Lett.*, 2012, **3**, 1351–1356.
12 Y. C. Choi, T. N. Mandal, W. S. Yang, Y. H. Lee, S. H. Im, J. H. Noh and S. I. Seok, *Angew. Chem., Int. Ed.*, 2014, **53**, 1329–1333.
13 Z. Li, X. Liang, G. Li, H. Liu, H. Zhang, J. Guo, J. Chen, K. Shen, X. San, W. Yu, R. E. I. Schropp and Y. Mai, *Nat. Commun.*, 2019, **10**, 125.
14 D.-B. Li, X. Yin, C. R. Grice, L. Guan, Z. Song, C. Wang, C. Chen, K. Li, A. J. Cimaroli, R. A. Awni, D. Zhao, H. Song, W. Tang, Y. Yan and J. Tang, *Nano Energy*, 2018, **49**, 346–353.
15 G. Li, Z. Li, X. Liang, C. Guo, K. Shen and Y. Mai, *ACS Appl. Mater. Interfaces*, 2018, **11**, 828–834.
16 X. Wen, C. Chen, S. Lu, K. Li, R. Kondrotas, Y. Zhao, W. Chen, L. Gao, C. Wang, J. Zhang, G. Niu and J. Tang, *Nat. Commun.*, 2018, **9**, 2179.
17 M. A. Tumelero, R. Faccio and A. A. Pasa, *J. Phys. Chem. C*, 2016, **120**, 1390–1399.
18 X. Liu, X. Xiao, Y. Yang, D.-J. Xue, D.-B. Li, C. Chen, S. Lu, L. Gao, Y. He, M. C. Beard, G. Wang, S. Chen and J. Tang, *Prog. Photovoltaics*, 2017, **25**, 861–870.

19 J. D. Gouveia and J. Coutinho, *Electronic Structure*, 2019, **1**, 015008.
20 G. Kresse and J. Hafner, *Phys. Rev. B: Condens. Matter Mater. Phys.*, 1993, **47**, 558–561.
21 G. Kresse and J. Hafner, *Phys. Rev. B: Condens. Matter Mater. Phys.*, 1994, **49**, 14251–14269.
22 G. Kresse and J. Furthmüller, *Phys. Rev. B: Condens. Matter Mater. Phys.*, 1996, **54**, 11169–11186.
23 G. Kresse and J. Furthmüller, *Comput. Mater. Sci.*, 1996, **6**, 15–50.
24 A. V. Krukau, O. A. Vydrov, A. F. Izmaylov and G. E. Scuseria, *J. Chem. Phys.*, 2006, **125**, 224106.
25 S. Grimme, *J. Comput. Chem.*, 2004, **25**, 1463–1473.
26 M. Birkett, W. M. Linhart, J. Stoner, L. J. Phillips, K. Durose, J. Alaria, J. D. Major, R. Kudrawiec and T. D. Veal, *APL Mater.*, 2018, **6**, 084901.
27 C. Freysoldt, J. Neugebauer and C. G. Van de Walle, *Phys. Rev. Lett.*, 2009, **102**, 016402.
28 S. Lany and A. Zunger, *Phys. Rev. B: Condens. Matter Mater. Phys.*, 2008, **78**, 235104.
29 S. T. Murphy and N. D. M. Hine, *Phys. Rev. B: Condens. Matter Mater. Phys.*, 2013, **87**, 094111.
30 K. Momma and F. Izumi, *J. Appl. Crystallogr.*, 2011, **44**, 1272–1276.
31 D. Wickramaratne, C. E. Dreyer, B. Monserrat, J.-X. Shen, J. L. Lyons, A. Alkauskas and C. G. V. de Walle, *Appl. Phys. Lett.*, 2018, **113**, 192106.
32 J. E. Lowther, *J. Phys. C: Solid State Phys.*, 1980, **13**, 3681–3696.
33 D. Han, Y. Y. Sun, J. Bang, Y. Y. Zhang, H.-B. Sun, X.-B. Li and S. B. Zhang, *Phys. Rev. B: Condens. Matter Mater. Phys.*, 2013, **87**, 155206.
34 S. Chen, A. Walsh, X.-G. Gong and S.-H. Wei, *Adv. Mater.*, 2013, **25**, 1522–1539.
35 S. Kim, J.-S. Park and A. Walsh, *ACS Energy Lett.*, 2018, **3**, 496–500.
36 T. Gershon, Y. S. Lee, R. Mankad, O. Gunawan, T. Gokmen, D. Bishop, B. McCandless and S. Guha, *Appl. Phys. Lett.*, 2015, **106**, 123905.
37 T. Gershon, B. Shin, N. Bojarczuk, M. Hopstaken, D. B. Mitzi and S. Guha, *Adv. Energy Mater.*, 2015, **5**, 1400849.
38 D. Tiwari, T. Koehler, X. Lin, R. Harniman, I. Griffiths, L. Wang, D. Cherns, R. Klenk and D. J. Fermin, *Chem. Mater.*, 2016, **28**, 4991–4997.
39 R. E. Brandt, V. Stevanović, D. S. Ginley and T. Buonassisi, *MRS Commun.*, 2015, **5**, 265–275.
40 A. Zakutayev, C. M. Caskey, A. N. Fioretti, D. S. Ginley, J. Vidal, V. Stevanovic, E. Tea and S. Lany, *J. Phys. Chem. Lett.*, 2014, **5**, 1117–1125.
41 A. Walsh and A. Zunger, *Nat. Mater.*, 2017, **16**, 964–967.
42 A. Walsh, D. J. Payne, R. G. Egdell and G. W. Watson, *Chem. Soc. Rev.*, 2011, **40**, 4455–4463.
43 K. K. Bass, L. Estergreen, C. N. Savory, J. Buckeridge, D. O. Scanlon, P. I. Djurovich, S. E. Bradforth, M. E. Thompson and B. C. Melot, *Inorg. Chem.*, 2017, **56**, 42–45.
44 A. M. Ganose, S. Matsumoto, J. Buckeridge and D. O. Scanlon, *Chem. Mater.*, 2018, **30**, 3827–3835.
45 T. L. Hodgkins, C. N. Savory, K. K. Bass, B. L. Seckman, D. O. Scanlon, P. I. Djurovich, M. Thompson and B. Melot, *Chem. Commun.*, 2019, **55**, 3164–3167.
46 R. E. Brandt, J. R. Poindexter, P. Gorai, R. C. Kurchin, R. L. Z. Hoye, L. Nienhaus, M. W. B. Wilson, J. A. Polizzotti, R. Sereika, R. Žaltauskas, L. C. Lee, J. L. MacManus-Driscoll, M. Bawendi, V. Stevanović and T. Buonassisi, *Chem. Mater.*, 2017, **29**, 4667–4674.
47 R. C. Kurchin, P. Gorai, T. Buonassisi and V. Stevanović, *Chem. Mater.*, 2018, **30**, 5583–5592.
48 D. O. Scanlon, P. D. C. King, R. P. Singh, A. de la Torre, S. M. Walker, G. Balakrishnan, F. Baumberger and C. R. A. Catlow, *Adv. Mater.*, 2012, **24**, 2154–2158.